Electronic, magnetic and elastic properties of γ-Fe4X (X=B/C/N) from density functional theory calculations

ARTICLE *in* JOURNAL OF MAGNETISM AND MAGNETIC MATERIALS · MAY 2013

Impact Factor: 1.97 · DOI: 10.1016/j.jmmm.2012.12.044

7 AUTHORS, INCLUDING:

Zhiqing Lv
Yan Shan University
31 PUBLICATIONS **246** CITATIONS
SEE PROFILE

Wan-tang Fu
Yan Shan University
55 PUBLICATIONS **374** CITATIONS
SEE PROFILE

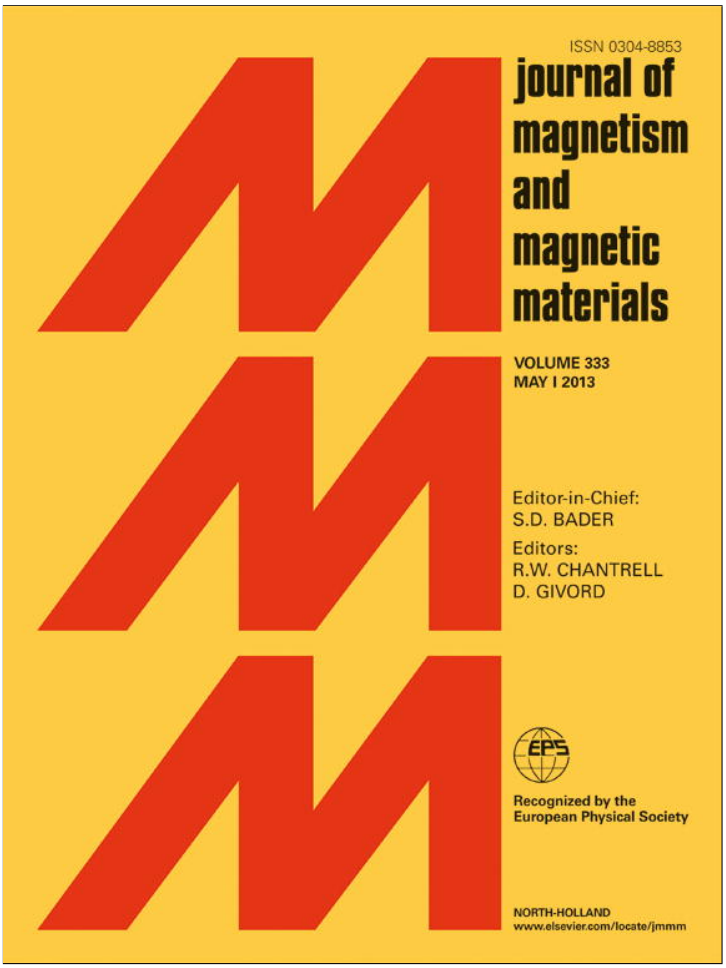

Journal of Magnetism and Magnetic Materials 333 (2013) 39–45

Contents lists available at SciVerse ScienceDirect

Journal of Magnetism and Magnetic Materials

journal homepage: www.elsevier.com/locate/jmmm

Electronic, magnetic and elastic properties of γ-Fe_4X (X=B/C/N) from density functional theory calculations

Z.Q. Lv [a,b], Y. Gao [a], S.H. Sun [c], M.G. Qv [a], Z.H. Wang [a], Z.P. Shi [a], W.T. Fu [a,*]

[a] State Key Laboratory of Metastable Material Science and Technology, Yanshan University, Qinhuangdao 066004, China
[b] Key Laboratory of Advanced Forging & Stamping Technology and Science, Ministry of Education of China, Yanshan University, Qinhuangdao 066004, China
[c] College of Science, Yanshan University, Qinhuangdao 066004, China

ARTICLE INFO

Article history:
Received 15 October 2012
Received in revised form
17 December 2012
Available online 2 January 2013

Keywords:
γ phase
Magnetic property
Elastic property
First-principle
Crystal structure

ABSTRACT

The crystal structure and elastic and electronic properties of γ-Fe_4B were predicted using density functional theory calculations. In view of the formation energy, the phase stability increases from γ-Fe_4B, γ-Fe_4C to γ-Fe_4N. It is confirmed that the bonds of γ-Fe_4X (X=B/C/N) are complex mixtures of metallic, covalent and ionic characters. The ionicity of Fe–X increases from Fe–B, Fe–C to Fe–N in γ-Fe_4X (X=B/C/N). The magnetic moments of γ-Fe_4X (X=B/C/N) are mainly contributed by 3d electrons of metal atoms. For γ-Fe_4B, the values of Fe Ms are 3.118 and 2.024 μ_B for FeI and FeII, respectively. For γ-Fe_4C, the values of Fe Ms are 3.135 and 1.696 μ_B for FeI and FeII, respectively. For γ-Fe_4N, the values of Fe Ms are 2.972 and 2.307 μ_B for FeI and FeII, respectively. The Debye temperatures of γ-Fe_4X (X=B/C/N) are predicted as 366, 500 and 477 K.

1. Introduction

The effects on the properties of steels and alloys of interstitial atoms are of scientific interest and industrial value. Interstitial atoms (such as C, N, B, etc.) play an important role in steels and alloys, which are mainly in interstitial sites of solid solution (such as γ phase, α phase, etc.) or forms interstitial phases with metal atoms (such as carbides, nitrides, borides, etc.). Many experimental and theoretical studies have been carried out on the crystal structures and properties of the interstitial solid solutions (such as γ phase, α phase, etc.) [1–5] and interstitial phases (such as carbides, nitrides, borides, etc.) in steels [6–11]. Kong and co-workers [1] studied the effects of interstitial atoms (H/C/N) on the magnetic properties of γ-Fe using the spin-polarized linear muffin-tin orbitals method. Their results indicated the insertion of the interstitial atoms changed the Fe–Fe interaction and Fe–Z (Z=H/C/N) interaction. Matar et al. [2] calculated the potential existence of anti-postperovskite iron nitride Fe_4N and obtained the equations of states for state for cubic anti-postperovskite and hypothetic anti post-postperovskite forms of Fe_4N within DFT for the spin-polarized and non-magnetic configurations. Peltzer et al. [3] investigated the electronic structure of FCC-Fe_nX (X=C, N; n=4, 8) alloys by the full-potential linear augmented-plane wave (FLAPW) method. Their results indicated that the magnetic phase was more stable than the non-magnetic one for both Fe–C and Fe–N solid solution. Deng et al. [4] studied the structure and stability of Fe_4C bulk and surface using the density functional theory calculations. They found that the structure with octahedral interstitial carbon was more stable than that with tetrahedral interstitial carbon. Fang et al. [5] calculated the formation energy of γ-Fe_4C, and confirmed the stability relationship between γ-Fe_4C and other iron carbides in steels. Fang and co-workers [6] studied the structures and electronic properties of Fe_2C and Fe_2N using the density functional theory within the projector-augmented wave method (PAW), and the formation energies of Fe_2X (X=C/N) were calculated, but the borides with hexagonal structure were not referred to. Jang and co-workers [7] calculated the stability of ε carbides by the use of the full-potential linearized augmented-plane-waves method (PLAPW), and confirmed ε-carbide instability. Kong and Li [8] investigated the cohesive energy and local magnetic properties of Fe_3B using the self-consistent linear muffin-tin orbitals (LMTO) method, and the magnetic properties and Curie temperature of θ-Fe_3B were obtained. Lv and coworkers [9] calculated the mechanical and magnetic properties of ε-Fe_2C and η-Fe_2C using the density functional theory, and indicated the stability relationship between ε-Fe_2C and η-Fe_2C. Recently, Wang and coworkers [10,11] performed the first-principles calculations of the electronic and magnetic properties of alloyed cementite (Co/Ni/Cr/Mn), and orthorhombic structures and the differences between them were also investigated. Though a lot of work has been done up to data, there are still a few questions in this field to be clarified. For instance, the effects of B adding into γ-Fe on the elastic and electronic properties of the γ-phase are not clear, and the reasons that insertion of B/C/N in Fe induces remarkable changes of the properties of steels are as yet unknown.

The present study aims to examine the structural, electronic and magnetic properties of γ-Fe_4X (X=B/C/N) and to clarify the

* Corresponding author. Tel.: +86 335 8074036; fax: +86 335 805 7068.
E-mail addresses: zqlv@ysu.edu.cn (Z.Q. Lv), wtfu@ysu.edu.cn (W.T. Fu).

0304-8853/$ - see front matter © 2012 Elsevier B.V. All rights reserved.
http://dx.doi.org/10.1016/j.jmmm.2012.12.044

relationship between them using the first-principles method. The formation energies of γ-Fe_4X (X=B/C/N) are calculated and compared. We also investigated the elastic properties, thermal stability and Debye temperatures (θ_D) of γ-Fe_4X (X=B/C/N).

2. Crystal structure and calculation details

The first-principle code CASTEP (Cambridge Serial Total Energy Package) [12], which employs the density functional theory (DFT) within the pseudo-potential plane–wave method [13,14], was used for all calculations. The exchange-correlation potential was evaluated using the Perdew–Burke–Ernzerhof function [15] within the generalized gradient approximation (PBE-GGA) [16]. The interactions between the core and valence electrons were described by ultra-soft pseudo-potentials [17], and the Kohn–Sham one-electron states were expanded in a plane wave basis set-up to 400 eV. The energy calculations in the first irreducible Brillouin zone were conducted by using $7\times7\times7$ k-point grid of Monkhorst–Pack scheme [18]. The convergence criteria for structure optimization and energy calculation were set to fine quality with the tolerance for the stress concentration factor (SCF), energy, maximum force and maximum displacement of 10^{-6} eV/atom, 10^{-5} eV/atom, 0.03 eV/Å and 0.001 Å, respectively. Because of its large effect on magnetic systems, spin polarization was included in the calculations to correctly account for its magnetic properties. After getting equilibrium geometry, the elastic constants were obtained using the stress–strain method [19,20].

The structures and formation energies are addressed in Section 3.1. Details of the electronic and magnetic properties of γ-Fe_4X (X=B/C/N) are analyzed in Section 3.2. The elastic properties and Debye temperatures of γ-Fe_4X (X=B/C/N) are calculated in Section 3.3 and Section 3.4, respectively.

3. Results and discussions

3.1. Structures and formation energies

The γ-Fe crystallizes in the cubic space group Fm-3m (S.G. no. 225) with four Fe atoms per unit cell. Two different Fe environments are distinguished: the corner sites (FeI) and the face-centered sites (FeII) [21]. The γ-Fe_4X (X=B/C/N) crystallizes in the same structure with γ-Fe, with interstitial atoms (such as B, N, C, etc.) in the octahedral interstice of γ-Fe. A three-dimensional drawing of the unit cell is shown in Fig. 1.

The ground-state properties of the γ-Fe_4X (X=B/C/N) were investigated from their total energy, which is calculated as a function of volume. According to the Murnaghan equation of state [22], the equilibrium lattice constants and atomic positions can be obtained (see Table 1). It can be found that the calculated values of the lattice constants match fairly well with the experimental ones [5,23,24] and other calculations [1,4,25]. The lengths of Fe–X bonds in γ-Fe_4X (X=B/C/N) are 1.9027, 1.8739 and 1.8899 Å, respectively. The length of Fe–C is smallest in them.

The formation enthalpy (ΔE) of γ-Fe_4X (X=B/C/N) from the elements (α-Fe, graphite, α-boron, and molecular N_2) can be described as

$$\Delta E = E(Fe_4X) - 4E(Fe) - E(X) \quad (1)$$

At $T=0$ K and $p=0$ Pa, the formation enthalpy equals the calculated formation energy (ΔE), i.e., $\Delta H(Fe_4X) = \Delta E(Fe_4X)$, when the zero-vibration contribution is ignored [5,6,10]. The formation enthalpy (energy) defined in this way can be used to measure the thermodynamic stability of Fe_4X with respect to the α-Fe, graphite, α-boron, and molecular N_2. The formation energies of

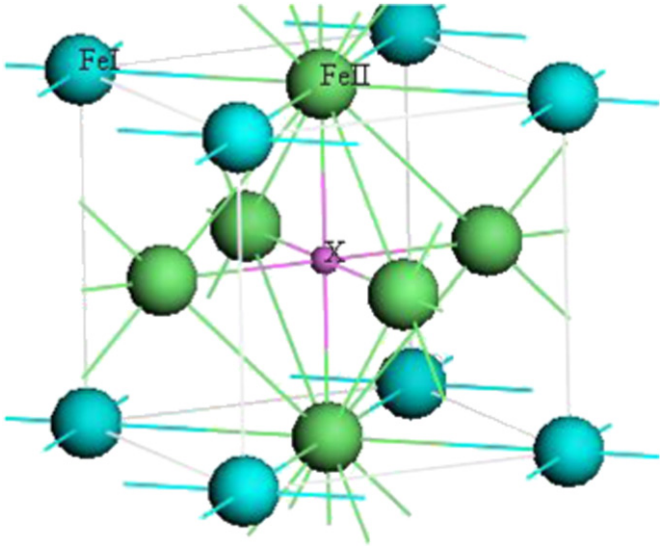

Fig. 1. Crystal structure of γ-Fe_4X (X=B/C/N), showing the fcc Fe lattice and X atom in the octahedral sites.

Table 1
Experimental (values within brackets) and calculated lattice constants a_0, b_0, c_0 (Å), v_0 (Å^3), ρ(g/cm^3) and the bond length of γ-Fe_4B, γ-Fe_4C and γ-Fe_4N.

	Fe_4B	Fe_4C	Fe_4N
A=b=c	3.817	3.748 (3.740[a])	3.780 (3.792[b])
$A=\beta=\gamma$	90	90	90
v	55.63	52.64	54.00
ρ	6.991	7.426	7.300
Fe–Fe	2.6993	2.6500	2.6727
Fe–C	1.9027	1.8739	1.8899

[a] Ref. [4],
[b] Ref. [23]

γ-Fe_4X (X=B/C/N) are 0.074, −0.15, 0.097 eV/atom, respectively. In view of the formation energy, the phase stability increases from γ-Fe_4B, γ-Fe_4C to γ-Fe_4N. The formation energy of γ-Fe_4N is negative, which indicates that the formation of γ-Fe_4N is easier than γ-Fe_4B and γ-Fe_4C in iron alloys. The formation energies of γ-Fe_4B and γ-Fe_4C are positive, which indicates that the two phases are unstable at ambient conditions. The formation energy of γ-Fe_4N is close to other calculations [3,8].

3.2. Electronic and magnetic properties of phases

In this part, the electronic structures of these γ-phases will be discussed and compared with each other. Fig. 2 shows the calculated total density of states (tDOS) for γ-Fe_4X (X=B/C/N). Fig. 3 depicts the details of the partial densities of states (pDOS) of atoms in γ-Fe_4X (X=B/C/N).

As shown in Fig. 2, the electronic structures of γ-Fe_4X (X=B/C/N) display similarities. The Fermi level is at 0 eV for all the data in this present work. There are no energy gaps near to the Fermi level, which shows a metallic nature of γ-Fe_4X (X=B/C/N). The valence bands are composed of two separate parts. At the lower energy range, the semicore B/C/N 2s states from a broad band of about 3.9 eV/3 eV/1.8 eV. Boron's 2s band lies at −6.7 and −10.6 eV, Carbon's 2s band ranges from −11 to −14 eV and Nitrogen's 2s band is located at −17.8 and −16 eV. The shapes of the B/C/N 2s bands are almost identical for both spin-up and spin-down electrons. The widths of the B/C/N 2s states indicate the strong X–X interactions, as well as contributions to valence interactions, although they are semicore electrons [6]. The Fe's

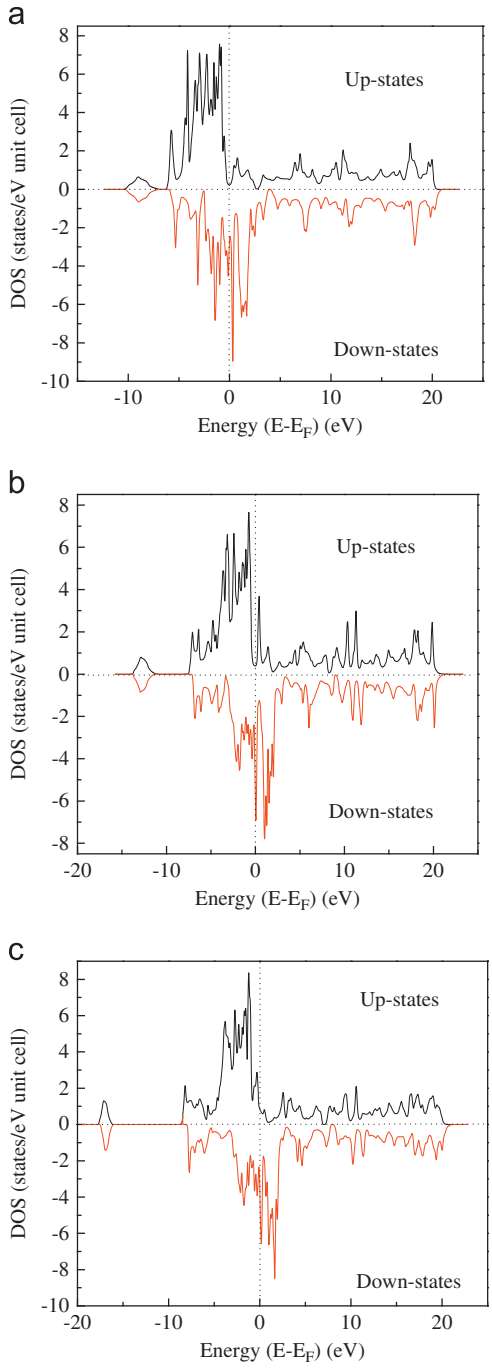

Fig. 2. Calculated spin-polarized total density of states of (a) γ-Fe_4B, (b) γ-Fe_4C and (c) γ-Fe_4N.

4s states are affected by the 2s band of the X (B/C/N) atom, their distributions accord with B/C/N atoms in γ-Fe_4X (X=B/C/N) and their contribution are much smaller than X 2s states. There is an energy gap between the X 2s states and the upper-energy bands in γ-Fe_4X (X=B/C/N), which are composed of mainly X 2p and Fe 3d states. The energy gaps between the lower valence bands and the upper valence bands are 0.5, 3.5 and 7 eV for γ-Fe_4B, γ-Fe_4C and γ-Fe_4N, respectively. This indicates that the chemical bonds of γ-Fe_4X (X=B/C/N) take on ionicity and the ionicity of Fe–X strengthens from Fe–B, Fe–C to Fe–N. From about -6.2 to -5 eV, there exists the hybridization of B 2p and Fe 3d for γ-Fe_4B. From about -7.6 to -4.5 eV, there exists the hybridization of C 2p and Fe 3d for γ-Fe_4C. From about -8.5 to -5 eV, there exists the hybridization of N 2p and Fe 3d for γ-Fe_4N.

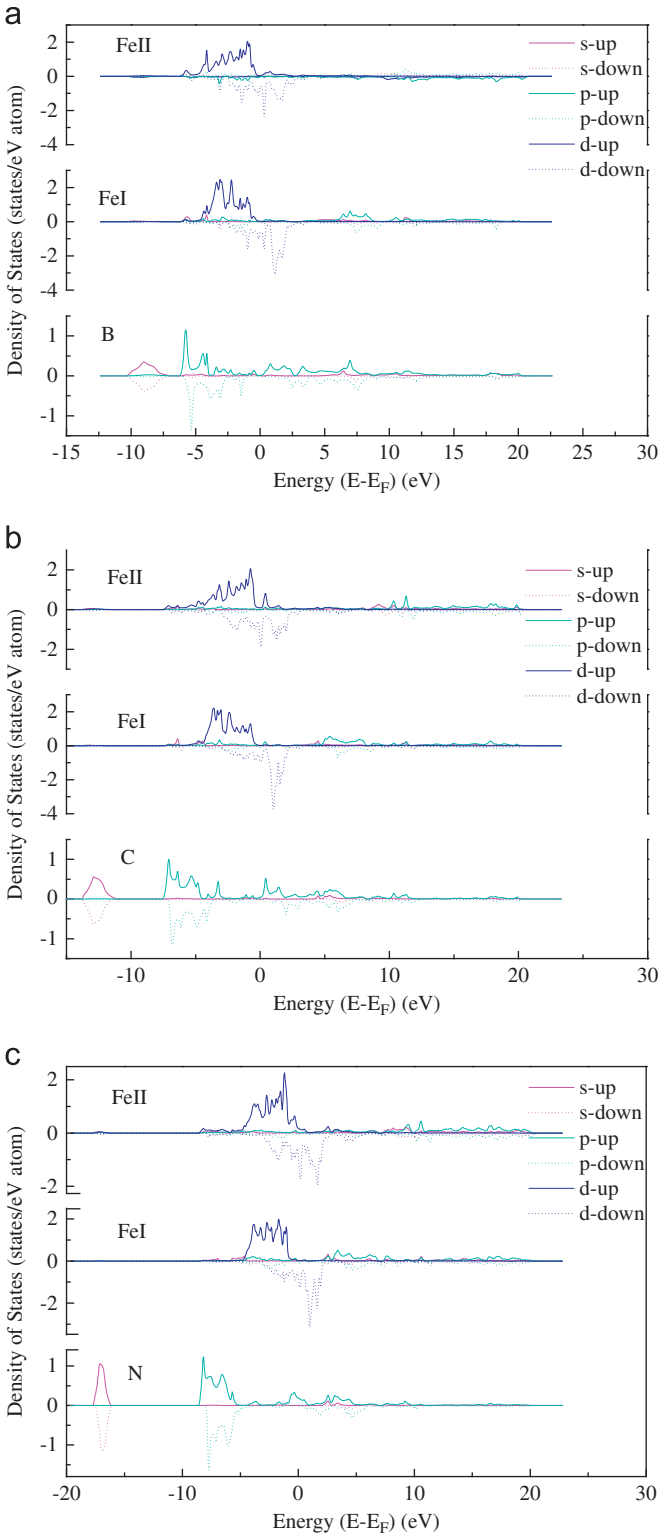

Fig. 3. Calculated spin-up and spin-down partial density of states of (a) γ-Fe_4B, (b) γ-Fe_4C and (c) γ-Fe_4N.

Near the Fermi level, the calculated DOS profiles of these phases are dominated by Fe's 3d bands in γ-Fe_4X (X=B/C/N). In addition, the unoccupied states are dominated by Fe 3d and X 2p states, as shown in Figs. 2 and 3, and they indicate that there are strong covalent features between B/C/N 2p and Fe 3d [26].

Contour plots of electron density distributions are useful for detailed analysis of the chemical bonds and the charge transfer in

a compound. As shown in Figs. 4 and 5, the electron density distribution map of the plane with Fe and X (B, C, N) atoms is plotted in two ways: the total density map (Fig. 4) and the electron density difference map (Fig. 5). The electron density difference was determined as $\Delta\rho = \{\rho_{\text{crystal}} - \sum \rho_{\text{at}}\}$, where $\rho_{crystal}$ and ρ_{at} are the valence electron densities for γ-Fe_4X (X=B/C/N) and the corresponding free atoms, respectively.

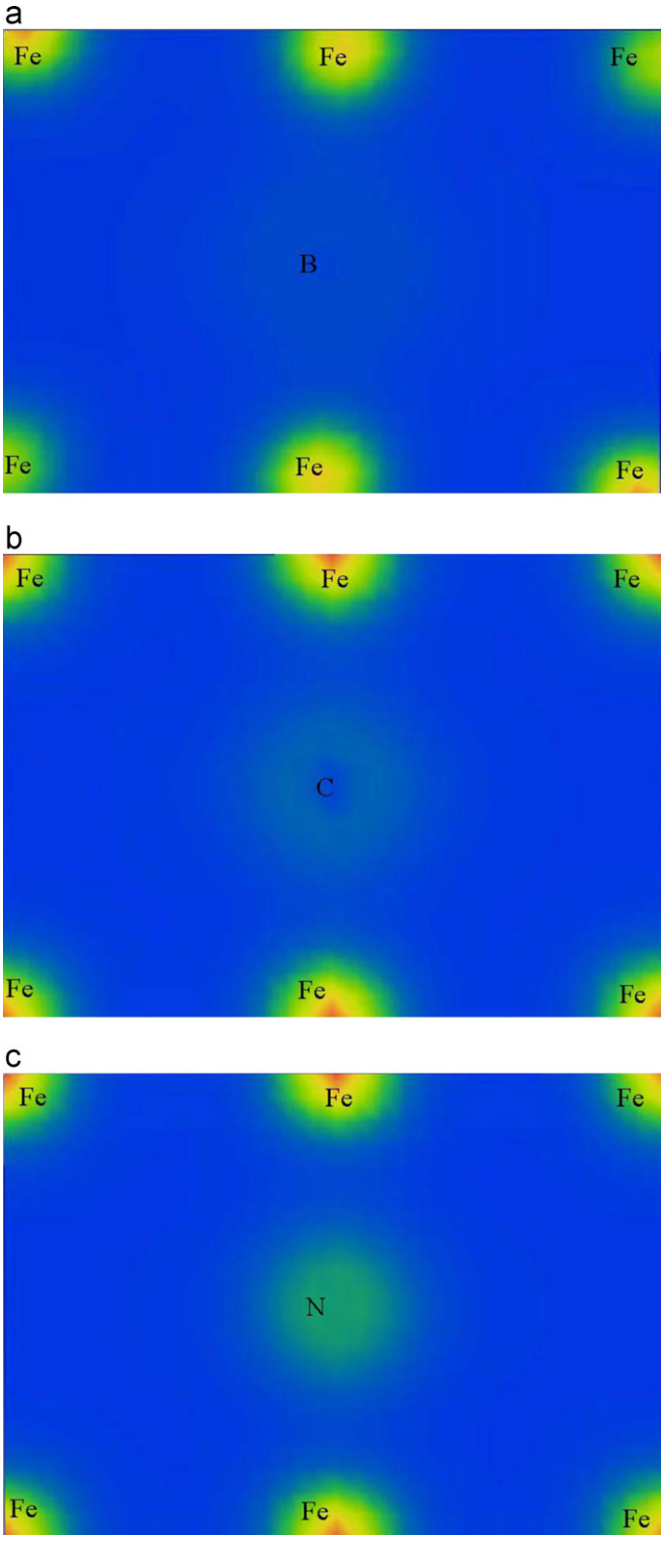

Fig. 4. Total electron density map of the plane (111) with Fe–X bonds of γ-Fe_4X (X=B/C/N) plotted from 0 (blue) to 15 (red) e $Å^{-3}$ (a) γ-Fe_4B, (b) γ-Fe_4C and (c) γ-Fe_4N. (For interpretation of the references to color in this figure legend, the reader is referred to the web version of this article.)

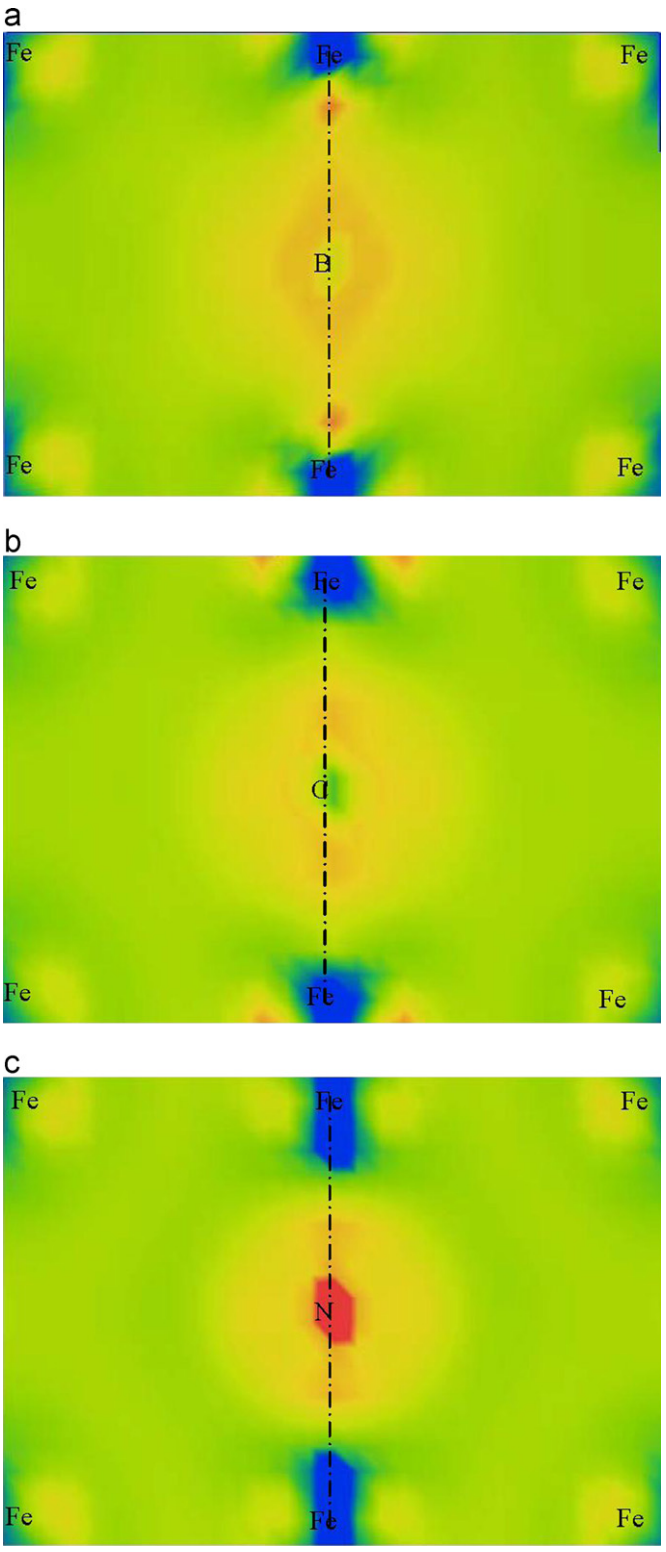

Fig. 5. Electron density difference map of the plane (111) with Fe–X bonds of γ-Fe_4X (X=B/C/N) plotted from −0.2 (blue) to 0.2 (red) e $Å^{-3}$ (a) γ-Fe_4B, (b) γ-Fe_4C and (c) γ-Fe_4N. (For interpretation of the references to color in this figure legend, the reader is referred to the web version of this article.)

There is strong similarity in the contour plots of γ-Fe_4X (X=B/C/N), particularly at Fe sites (labeled by blue crosses) in Fig. 4. The densities around the Fe sites and B/C/N sites are almost

spherical. The core regions of X (X=B, C, N) and Fe have the largest density from Fig. 4, which are mainly due to ionic core orbits. Clearly, the density at N is much bigger than that the B/C sites. That is due to the fact that there is one more 2p electron at each N ($2s^2 2p^3$) atom than at the B ($2s^2 2p^1$) and C ($2s^2 2p^2$) sites. Overlaps occur between the electron densities of Fe and X, which indicates the chemical bonding between Fe and B/C/N. The delocalized electron clouds represent the metallic bonds between the metal atoms and the highest energy level near the Fermi surface being occupied. As shown in Fig. 5, the electron densities near the Fe atom decrease and the electron densities of nonmetal (B/C/N) atoms increase. There exist the loss and gain of electrons between the Fe atom and the X atom along the Fe–X direction. The ionicity of Fe–X increases from Fe–B, Fe–C to Fe–N. This result accords with the DOS analyses (Figs. 2 and 3). In the interstitial regions, the increment of delocalized electrons is attributed to the metallic bonds.

The calculated length of the Fe–B bond is 1.9027 Å, and the corresponding overlapping population value is 0.57 in γ-Fe_4B. The calculated length of the Fe–C bond is 1.8739 Å, and the corresponding overlapping population value is 0.65 in γ-Fe_4C. The length of the Fe–N bond is 1.8899 Å, and the corresponding overlapping population value is 0.62 in γ-Fe_4N. This indicates that strong covalent bonding states exist in γ-Fe_4X (X=B/C/N). This results accords with the above analyses of electron densities in γ-Fe_4X (X=B/C/N). From the analyses of electronic structure, the bonds nature of γ-Fe_4X (X=B/C/N) may be described as a mixture of covalent-ionic, due to the d-resonance in the vicinity of the Fermi level, and partly metallic. This similar to the characters of bonds in Fe_3X (X=B/C/N) [26,27].

The γ-Fe_4B, γ-Fe_4C and γ-Fe_4N were calculated to be ferromagnetic. As shown in Figs. 2 and 3, there are large differences for the DOSs at the Fermi level for the spin-up ($n_\uparrow[E_F]$) and the spin-down ($n_\downarrow[E_F]$). For γ-Fe_4B, $n_\uparrow[E_F]$ is 0.22 states/eV per formula unit, and $n_\downarrow[E_F]$=2.52 states/eV per formula unit. For γ-Fe_4C, $n_\uparrow[E_F]$ is 0.39 states/eV per formula unit, and $n_\downarrow[E_F]$=6.01 states/eV per formula unit. For γ-Fe_4N, $n_\uparrow[E_F]$ is 0.84 states/eV per formula unit, and $n_\downarrow[E_F]$=3.48 states/eV per formula unit. Therefore, the spin polarization $P=\{[n_\uparrow(E_F)-n_\downarrow(E_F)]/[n_\uparrow(E_F)+n_\downarrow(E_F)]\}=84\%$ for γ-Fe_4B, $P=88\%$ for γ-Fe_4C and $P=61\%$ for γ-Fe_4N. From Fig. 3, the spin moments of each atom and contribution of each electron shell were calculated, which are listed in Table 2. The average magnetic moment of γ-Fe_4B, γ-Fe_4C and γ-Fe_4N are 8.93, 8.10 and 10.1 μ_B/unit, respectively. The results of Fe_4C and Fe_4N are similar to that in the literatures [1,3,4]. The differences of Ms between Fe_4X mainly result from that of the spin density difference of Fe and X (X=B/C/N) in the three crystals (see Fig. 3). For γ-Fe_4B, the values of Fe Ms are 3.118 and 2.024 μ_B for FeI and FeII, respectively. For γ-Fe_4C, the values of Fe Ms are 3.135 and 1.696 μ_B for FeI and FeII, respectively. For γ-Fe_4N, the values of Fe Ms are 2.972 and 2.307 μ_B for FeI and FeII, respectively. For γ-Fe_4C and γ-Fe_4N, the calculated magnetic moments are in agreement with previous studies [4,24,28]. From Table 2, it can also be seen the magnetic moments of γ-Fe_4X (X=B/C/N) are mainly contributed by 3d electrons of metal atoms. The contributions of s and p electrons are mostly negative to the magnetism of γ-Fe_4X (X=B/C/N).

3.3. Elastic properties of phases

The mechanical stability of a crystal implies that the strain energies are positive. The mechanical stability of the crystal is described with elastic constants C_{ij} depending on the crystal structure. For the cubic crystal structures such as γ-phase, there are three different symmetry elements (C_{11}, C_{12}, C_{44}). The stability criteria for a cubic crystal are [29]

$$C_{11}>0,\ C_{11}-C_{12}>0,\ C_{44}>0,\ C_{11}+2C_{12}>0 \quad (2)$$

As shown in Table 3, the elastic constants C_{ij} of γ-Fe_4B, γ-Fe_4C and γ-Fe_4N were calculated at their equilibrium lattice constants and optimized structure. The calculated results of γ-Fe_4N are similar to that in the literature [30]. From the results, we can find γ-Fe_4X (X=B/C/N) are mechanically stable as their elastic constants satisfy with formula (2), respectively.

When single crystal samples cannot be obtained, it is impossible to measure the individual elastic constants C_{ij}. Instead, the isotropic bulk modulus B and shear modulus G are determined [31]. These quantities cannot in general be calculated directly from the C_{ij}, but we can use our values to place bounds on the isotropic moduli. Reuss found lower bounds for all lattices [32], while Voigt discovered upper bounds [33]. Hill [34] showed that the Voigt and Reuss averages were limits and suggested that the actual effective moduli could be approximated by the arithmetic mean of the two bounds.

The calculated Voigt's bulk modulus (B_v), Reuss's bulk modulus (B_R), effective bulk modulus (B), Voigt's shear modulus (G_v), Reuss's shear modulus (G_R), and effective shear modulus (G) of γ-Fe_4B, γ-Fe_4C and γ-Fe_4N are given in Table 4.

The ratio of B to G gives us an estimation of the degree of ductility [35]. The ratios of γ-Fe_4X (X=B/C/N) are higher than the critical value 1.75, separating ductile and brittle behavior of a material. The bigger the ratio, the higher the ductility is. It can be

Table 3
Calculated elastic constants of γ-Fe_4B, γ-Fe_4C and γ-Fe_4N (C_{ij} in GPa).

	C_{11}	C_{12}	C_{44}
Fe_4B	322.1	100.2	18.1
Fe_4C	388.9	145.1	59.5
Fe_4N	322.8	132.0	48.3

Table 2
Calculated magnetic moments of each atom and unit cell.

Species	Fe_I (μ_B/atom)			Fe_{II} (μ_B/atom)			X (μ_B/atom)		Ms
	s	*p*	*d*	*s*	*p*	*d*	*s*	*p*	(μ/unit)
γ-Fe_4B	3.118			2.024			−0.324/B		8.93
	0.021	−0.137	3.233	−0.011	−0.126	2.161	−0.044	−0.280	
γ-Fe_4C	3.135 (3.12[a])			1.696 (1.74[a])			−0.200/C		8.10
	0.024	−0.109	3.218	−0.027	−0.114	1.836	−0.014	−0.185	
γ-Fe_4N	2.972 (2.90[b], 3.0[c])			2.307 (2.33[b], 2.0[c])			0.050/N		10.01
	−0.008	−0.161	3.141	−0.015	−0.105	2.428	−0.002	0.050	

[a] Ref. [4],
[b] Ref. [24],
[c] Ref. [28]

Table 4
Calculated Voigt's bulk modulus (B_v), Reuss's bulk modulus (B_R), effective bulk modulus (B), Voigt's shear modulus (G_v), Reuss's shear modulus (G_R), effective shear modulus (G) and Young's modulus (E in Gpa) for γ-Fe_4B, γ-Fe_4C and γ-Fe_4N.

	B_V	B_R	B	G_V	G_R	G	B/G
Fe_4B	174.2	174.2	174.2	55.2	27.2	41.2	4.23
Fe_4C	226.4	226.4	226.4	84.4	74.8	79.6	2.84
Fe_4N	195.6	195.6	195.6	67.1	60.2	63.6	3.08

seen that the three phases are ductile materials. This is in agreement with the nature of austenitic steels. The bulk modulus of γ-Fe_4B is smallest in the three phases, and the ductility of γ-Fe_4B (4.23) is better than that of γ-Fe_4X (X=C/N).

3.4. Calculation of Debye temperature

Debye temperature is an important fundamental parameter closely related to many physical properties such as elastic constants, specific heat, and melting temperature. One of the standard methods to calculate the Debye temperature (θ_D) is from elastic constants data, since θ_D may be estimated from the average sound velocity v_m by the following equation [36]:

$$\theta_D = \frac{h}{k_B}\left[\frac{3n}{4\pi V}\right]^{1/3} v_m \tag{3}$$

where h is Plank's constant, k_B is Boltzmann's constant, n is the number of atoms in cell and V is the cell volume. The average sound velocity in the polycrystalline material is given by [37]:

$$v_m = \left[\frac{1}{3}\left(\frac{2}{v_t^3}+\frac{1}{v_l^3}\right)\right]^{-1/3} \tag{4}$$

where v_l and v_t are the longitudinal and transverse sound velocity obtained using the shear modulus G and the bulk modulus B from Navier's equation [37]:

$$v_t = \left(\frac{3B+4G}{3\rho}\right)^{1/2} \text{ and } v_l = \left(\frac{G}{\rho}\right)^{1/2} \tag{5}$$

Heat capacity is an invaluable tool to explore the fundamental properties of materials as it probes low-lying excitations, and the experimental results can be directly compared to first-principle calculations. For metallic-like, three-dimensional materials at the lowest temperatures, the constant pressure heat capacity C_p can be approximated by the well-known relationship [38]:

$$Cp = \gamma T + \beta T^3 \tag{6}$$

where γ is related to the electron density of states and β relates to the phonon excitations. The γ term is given by [39]

$$\gamma = \frac{\pi^2 k_B^2 N(E_F)}{3} \tag{7}$$

where k_B is Boltzmann's constant. For the phonon contribution to Cp, the characteristic parameter typically reported is the Debye temperature θ_D, which is related to β by [39]

$$\theta_D^3 = \frac{4\pi^4 R}{5\beta} N \tag{8}$$

where N is the number of models per formula unit, R is the molar gas constant. The calculated sound velocity, Debye temperature γ and β of γ-Fe_4X (X=B/C/N) are given in Table 5. The Debye temperatures (θ_D) of γ-Fe_4X (X=B/C/N) are 366, 500, and 477 K, respectively. This indicates that the thermal stability of γ-Fe_4C is higher than γ-Fe_4X (X=B/N).

Table 5
Calculated longitudinal, transverse and average sound velocity (v_l, v_t, v_m in m/s) from polycrystalline elastic modulus, the Debye temperature (θ_D in K), average electronic heat capacity contribution (γ, in 10^{-2} J/mol K^2), and average phonon heat capacity contribution (β, in 10^{-5} J/mol K^4) for γ-Fe_4B, γ-Fe_4C and γ-Fe_4N.

	v_l	v_t	v_m	θ_D	γ	β
Fe_4B	5725	2428	2744	366	1.94	6.59
Fe_4C	6692	3274	3677	500	4.53	2.59
Fe_4N	6198	2952	3320	447	3.06	3.61

4. Conclusion

A complete theoretical analysis of the electronic, magnetic and elastic properties of γ-Fe_4X (X=B/C/N) has been presented by means of first-principle calculations. The calculated equilibrium structural parameters of γ-Fe_4C and γ-Fe_4N are in agreement with the experimental results. Using the same calculating method, the crystal structure of the γ-Fe_4B is predicted. In view of the formation energy, the phase stability increases from γ-Fe_4B, γ-Fe_4C to γ-Fe_4N. The formation energy of γ-Fe_4N is negative, which indicates that the formation of γ-Fe_4N is easier than other phases in the steels or Fe–N/B alloys. From the calculated results, it is confirmed that the bonds of γ-Fe_4X (X=B/C/N) are complex mixtures of metallic, covalent, and ionic characters. The ionicity of Fe–X increases from Fe–B, Fe–C to Fe–N in γ-Fe_4X (X=B/C/N). For γ-Fe_4B, the values of Fe Ms are 3.118 and 2.024 μ_B for FeI and FeII, respectively. For γ-Fe_4C, the values of Fe Ms are 3.135 and 1.696 μ_B for FeI and FeII, respectively. For γ-Fe_4N, the values of Fe Ms are 2.972 and 2.307 μ_B for FeI and FeII, respectively. The Debye temperatures (θ_D) of ε-Fe_3X (X=B/C/N) are predicted as 366, 500 and 477 K, respectively. This indicates that the thermal stability of γ-Fe_4C is higher than γ-Fe_4X (X=B/N).

Acknowledgments

This research was supported by the Natural Science Foundation of China (No. 51101137 and No. 51171161) and the Natural Science Foundation of Hebei Province of China (No. E2011203055).

References

[1] Y. Kong, R.J. Zhou, F.S. Li, Physical Review B 56 (1996) 5461.
[2] F. Mater, Gerard Demazeau, Naim Ouaini, Alain Largeteau, Solid State Sciences 12 (2010) 1131–1135.
[3] E.L. Peltzer, y Bianca, J. Desimoni, N.E. Christensen, Physica B: Condensed Matter (Amsterdam, Netherlands) 354 (2004) 341–344.
[4] C.M. Deng, C.F. Hou, L.L. Bao, X.R. Shi, Y.W. Li, J.G. Wang, H.J. Jiao, Chemical Physics Letters 448 (2007) 83–87.
[5] C.M. Fang, M.A. van Huis, B.J. Thijsse, H.W. Zandbergen, Physical Review B 85 (2012) 054116.
[6] C.M. Fang, M.A. van Huis, J. Jansen, H.W. Zandbergen, Physical Review B 84 (2011) 094102.
[7] Jae Hoon Jang, In Gee Kim, H.K.D.H. Bhadeshia, Scripta Materialia 63 (2010) 121.
[8] Yong Kong, Fashen Li, Physical Review B 56 (1997) 3153.
[9] Z.Q. Lv, S.H. Sun, P. Jiang, B.Z. Wang, W.T. Fu., Computational Materials Science 42 (2008) 692–697.
[10] C.X. Wang, Z.Q. Lv, W.T. Fu, Y. Li, S.H. Sun, B. Wang, Solid State Sciences 13 (2011) 1658–1663.
[11] Z.Q. Lv, W.T. Fu, S.H. Sun, et al., Journal of Magnetism and Magnetic Materials 323 (2011) 915–919.
[12] M.D. Segall, P.J.D. Lindan, M.J. Probert, C.J. Pichard, P.J. Hasnip, S.J. Clark, M.C. Payne, Journal of Physics: Condensed Matter 14 (2002) 2717.
[13] W. Kohn, L.J. Sham, Physical Review A 140 (1965) 1133.
[14] P. Hohenberg, W. Kohn, Physical Review B 136 (1964) 384.
[15] J.A. White, D.M. Bird, Physical Review B 50 (1994) 4954.
[16] J.P. Perdew, K. Burke, M. Ernzerhof, Physical Review B 77 (1996) 3865.
[17] D. Vanderbilt, Physical Review B 41 (1990) 7892.
[18] H. Jmonkhorst, J.D. Pack, Physical Review B 13 (1976) 5188.
[19] S. Tian, Materials Physical Properties, Beijing University of Aeronautics and Astronautics Press, Beijing, 2004.

[20] L. Fast, J.M. Wills, B. Johansson, O. Eriksson, Physical Review B 51 (1995) 17431.
[21] J. Haglund, A. Fernandez Guillermet, G. Grimvall, M. Korling., Physical Review B 48 (1993) 11685–11691.
[22] F.D. Murnaghan, Proceedings of the National Academy of Sciences of the United States of America 30 (1944) 244.
[23] H. Jacobs, D. Reckenbach, U. Zach Wieja, Journal of Alloys and Compounds 227 (1995) 10–17.
[24] K. Oda, H. Fujimura, H. Ino, Journal of Physics: Condensed Matter 6 (1994) 679.
[25] A.N. Timoshenevskii, V.A. Timosheevskii, B.Z. Yanchitsky, V.A. Yavna, Computational Materials Science 22 (2001) 99.
[26] Z.Q. Lv, W.T. Fu, S.H. Sun, Z.H. Wang, W. Fan, M.G. Qv, Solid State Sciences 12 (2010) 404.
[27] W.H. Zhang, Z.Q. Lv, Z.P. Shi, S.H. Sun, Z.H. Wang, W.T. Fu, Journal of Magnetism and Magnetic Materials 324 (2012) 2271–2276.
[28] Y. Jiraskova, S. Havlicek, O. Schneeweiss, V. Perina, C. Blawert, Journal of Magnetism and Magnetic Materials 234 (2001) 477.
[29] D.C. Wallace, Thermodynamics of Crystals, Wiley, New York, 1972 (Chapter 1).
[30] T. Gressmann, M. Wohlschlogel, S. Shang, U. Welzel, A. Leineweber, E.J. Mittemeijer, Z.K. Liu, Acta Materialia 55 (2007) 5833–5843.
[31] M.J. Mehl, B.M. Barry, D.A. Papaconstantopoulos, Intermetallic compounds: principle and practice, in: J.H. Westbrook, R.L. Fleischeir (Eds.), Principles, vol. I, Wiley, London, 1995, p. 195 (Chapter 9).
[32] A. Reuss, Z. Angew. Math. Mech. 8 (1929) 55.
[33] W. Voigt, Lehrbush der Kristallphysik, Taubner, Leipzig, 1928.
[34] R. Hill, Proceedings of the Physical Society of London A 65 (1952) 349.
[35] S.Q. Wu, Z.F. Hou, Z.Z. Zhu, Solid State Sciences 11 (2008) 251.
[36] V. Kanchana, G. Vaitheeswaran, A. Savane, A. Delin, Journal of Physics: Condensed Matter 18 (2006) 9615.
[37] E. Schreiber, O.L. Anderson, N. Soga, Elastic Constants and Their Measurements, McGraw-Hill, New York, 1973.
[38] M.K. Drulis, H. Drulis, S. Gupta, M.W. Barsoum, T. El-Raghy, Journal of Applied Physics 99 (2006) 093502.
[39] M.K. Drulis, H. Drulis, A.E. Hachemer, A. Ganguly, T. El-Raghy, M.W. Barsoum, Journal of Alloys and Compounds 433 (2007) 59.